Volume 2
Number 4
July 2025
Pages 659-840

RSC Pharmaceutics

rsc.li/RSCPharma

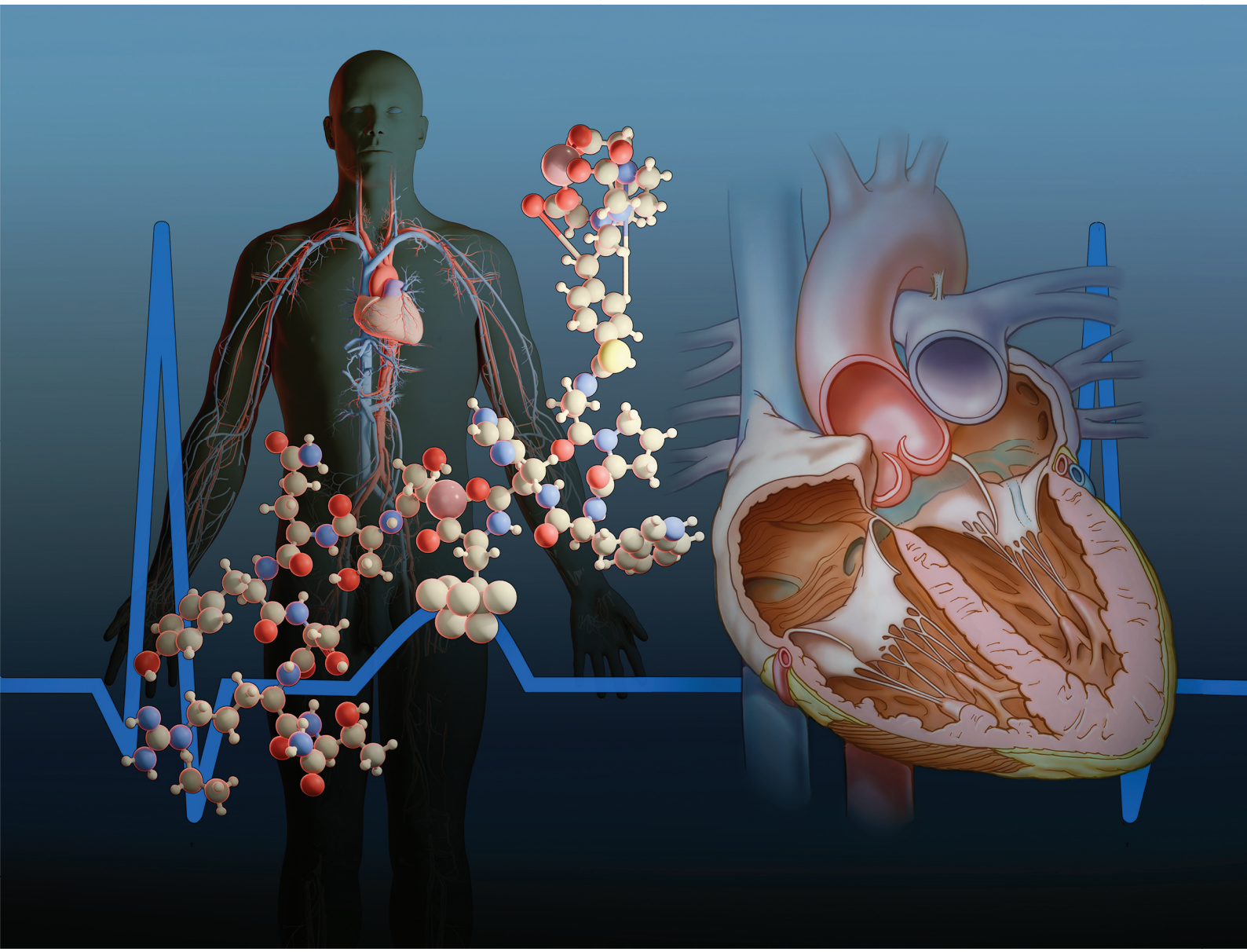

eISSN 2976-8713

ROYAL SOCIETY OF CHEMISTRY

PAPER

Mukesh K. Pandey *et al.*

Synthesis and preliminary evaluation of cardiac imaging with [^{68}Ga]Ga-NOTA-CTP in normal and infarcted CD1 mice

RSC Pharmaceutics

ROYAL SOCIETY OF CHEMISTRY

PAPER

View Article Online
View Journal | View Issue

Cite this: *RSC Pharm.*, 2025, **2**, 691

Synthesis and preliminary evaluation of cardiac imaging with [^{68}Ga]Ga-NOTA-CTP in normal and infarcted CD1 mice†

Surendra Reddy Gundam,[a] Manasa Kethamreddy,[a] Andy González Rivera,[a] Aditya Bansal,[a] Viktoria Krol,[a] Daniella A. Sahagun,[b] Joanna E. Kusmirek,[c] Derek R. Johnson,[a] Maliha Zahid,[b] Val J. Lowe[a] and Mukesh K. Pandey *[a,d,e]

Cell-penetrating peptide-based probes for positron emission tomography (PET) are currently being developed for cardiac imaging. Herein, we have conjugated a synthetic 12 amino acids (NH_2-APWHLSSQYSRT-COOH) cardiac targeting peptide (CTP) with a NOTA chelator for ^{68}Ga labeling. The [^{68}Ga]Ga-NOTA-CTP was synthesized with a decay-corrected radiochemical yield of 68.9 ± 12.8% (n = 13) and molar activity (A_m) of 1.3 ± 0.5 GBq per μmol (n = 13). The tracer was evaluated in healthy and diseased CD1 mice with myocardial infarction following ligation of the left anterior descending artery. PET/CT imaging and *ex vivo* biodistribution revealed rapid (within 30 min) clearance of [^{68}Ga]Ga-NOTA-CTP from the blood through renal and hepatobiliary excretion pathways in both healthy and infarcted animals. The uptake of [^{68}Ga]Ga-NOTA-CTP in the heart of healthy and infarcted animals did not show any statistically significant difference for up to 120 min post-injection, but regional differences within healthy and infarcted hearts were detected with [^{68}Ga]Ga-NOTA-CTP by PET/CT imaging at early time points post-injection. Within a healthy heart, the left ventricle standardized uptake value (SUV) was lower than the right ventricle SUV at 10–30 min post-injection. This regional difference between the left and right ventricles was absent in the infarcted heart, likely due to post-ligation changes.

Received 15th February 2025,
Accepted 27th May 2025

DOI: 10.1039/d5pm00047e

rsc.li/RSCPharma

Introduction

Cardiovascular diseases (CVDs) are the leading cause of mortality in the world.[1–4] Globally, 523 million CVD cases and associated 18.6 million deaths were reported in 2019.[5] Numerous novel radiotracers in positron emission tomography (PET) and single-photon emission computed tomography (SPECT) are being explored in assessing myocardial perfusion, cardiac autonomic dysfunction, atherosclerotic plaques, cardiac metabolism, and viability.[6–16] Out of the two modalities, PET is preferred over SPECT due to its higher sensitivity, greater interpretive certainty, lower patient dosimetry, and shorter imaging protocol. Importantly, in the case of CVDs, PET can assess microvascular function by quantitatively measuring the myocardial blood flow at rest and peak stress.[17,18]

In clinical practice, PET imaging of cardiac perfusion allows the detection of cardiac abnormalities. The perfusion imaging is commonly performed with ^{13}N-ammonia ($T_{1/2}$ = 9.9 min), the potassium analog ^{82}Rb ($T_{1/2}$ = 76 s), or ^{15}O-water ($T_{1/2}$ = 2.05 min).[18–26] These perfusion markers have their strengths and weaknesses. Administered ^{13}N-ammonia is rapidly cleared from the blood with a first-pass extraction fraction of ~80% and is taken up by the heart, brain, liver, and kidneys.[19,20] The uptake of ^{13}N-ammonia is proportional to coronary blood flow; once taken up, the ^{13}N-ammonia is metabolically trapped in the cardiac cells as ^{13}N-glutamine.[19,20] In the case of ^{82}Rb, after administration, ^{82}Rb is rapidly cleared from the body with a first-pass extraction fraction of ~65% and is taken up primarily in the heart, lungs, and kidneys.[23,24] The uptake of ^{82}Rb in the myocardium is also dependent on blood flow, and once taken up, ^{82}Rb is actively transported into the cardiac cells through the Na^+/K ATPase pump.[23,24] As compared to ^{13}N-ammonia, images from ^{82}Rb scans are inferior in resolution and image quality due to the longer positron range of ^{82}Rubidium (8.6 mm) than ^{13}N-ammonia (2.53–5.4 mm).[18–22,25] The third perfusion marker, ^{15}O-water is taken up by the heart by passive diffusion with highest first-pass extraction fraction

[a]*Division of Nuclear Medicine, Department of Radiology, Mayo Clinic, Rochester, MN 55905, USA. E-mail: pandey.mukesh@mayo.edu*
[b]*Division of Comprehensive Cardiology, Department of Cardiovascular Medicine, Mayo Clinic, Rochester, MN 55905, USA*
[c]*Division of Cardiovascular Radiology, Department of Radiology, Mayo Clinic, Rochester, MN 55905, USA*
[d]*Department of Pharmacology, Mayo Clinic, Rochester, MN 55905, USA*
[e]*Mayo Clinic Comprehensive Cancer Center, Mayo Clinic, Rochester, MN 55905, USA*
† Electronic supplementary information (ESI) available. See DOI: https://doi.org/10.1039/d5pm00047e

(~100%).[26] The positron range of ^{15}O-water (4.14 mm) is between the positron range of ^{13}N-ammonia and ^{82}Rb and consequently the imaging quality is better than ^{82}Rb scans but inferior to ^{13}N-ammonia scans.[21]

Besides imaging quality, other factors need to be considered when choosing a cardiac perfusion tracer. An onsite cyclotron is required for producing ^{13}N-ammonia and ^{15}O-water due to their shorter half-life, whereas the shorter half-life of ^{82}Rb necessitates an onsite ^{82}Sr/^{82}Rb generator. Installing and maintaining an onsite cyclotron or generator can be prohibitive for many hospital sites.[18–22] For ease of use and ready availability of perfusion tracers, comparatively longer half-life radiotracers are desirable for broader adoption of PET-based myocardial perfusion imaging in imaging centers lacking onsite cyclotrons or generators. In this context, ^{18}F, with a half-life of 109.7 min and a positron range of 1.03 mm, and ^{68}Ga, with a half-life of 67.71 min and a positron range of 3.5 mm, are possible choices for PET radionuclides for developing perfusion markers.[21,27–30]

More recently, a promising myocardial perfusion marker, [^{18}F]F-flurpiridaz or BMS-747158-02, is emerging as an option in cardiac imaging.[31–33] It is based on the insecticide pyridaben, an inhibitor of the mitochondrial respiratory complex I, a complex of the electron transport chain in the mitochondria.[31] It has a first-pass extraction fraction of 94% with primary uptake in the liver, brain, heart, and kidneys.[32,33] It has shown encouraging results in phase 3 clinical trials as a perfusion marker for detecting coronary artery disease.[33] There are two other ^{18}F labeled perfusion markers, fluorodihydrorotenone ([^{18}F]FDHR)[34] derived from insecticide and *p*-fluorobenzyl triphenylphosphonium cation ([^{18}F]FBnTP)[35,36] derived from fungicide that are under investigation at the preclinical stage for their performance as perfusion marker. After administration, these are rapidly cleared from the blood, taken up in the heart in a perfusion-dependent manner, and trapped in the mitochondria of cardiomyocytes. Meanwhile the manuscript is being written [^{18}F]F-flurpiridaz has received food and drug administration's approval in the United States for evaluation of myocardial ischemia and infarction.

Zahid *et al.* reported a synthetic 12-amino acid cardiac targeting peptide (CTP), NH_2-APWHLSSQYSRT-COOH, specifically targeting cardiomyocytes.[37–41] The fluorophore-conjugated CTP could accumulate in the heart of Balb/C mice following retro-orbital intravenous injection.[37–39] In a different study, accumulation of Cy5.5 labeled CTP was observed in the heart in an isolated rat heart after perfusion in a Langendorff perfusion system.[40,41] Following encouraging results *in vivo* and *ex vivo* murine models, Zahid *et al.* tested CTP conjugated-amiodarone (antiarrhythmic drug) in guinea pig[42,43] and CTP-conjugated miRNA106a for treating hypertrophic human cardiomyocytes.[44] Authors delivered amiodarone to the heart of guinea pigs after intraperitoneal administration of the CTP-amiodarone complex with a functional response.[42,43] The ability of CTP to specifically enter cardiomyocytes has been replicated in multiple vertebrate species by at least four independent researchers around the world.[45–48]

The exact mechanism by which CTP peptide gets internalized in the Cardiomyocytes is not well understood, however we hypothesize that since it is a positively charged peptide at physiological pH, it could cross the cytoplasmic membrane of cardiomyocytes passively like other cell penetrating peptides and charged molecules.[49,50] It is known that lipophilic cations are capable of passive diffusion into the cytoplasm and mitochondria of cardiomyocytes in response to a large negative plasma- and mitochondrial- membrane potentials.[50,51]

Encouraged by previous studies using CTP, an attempt was made to assess if radiolabeled CTPs can be used to image the heart. In this pursuit, the biodistribution of ^{99m}Tc radiolabeled CTP as a [^{99m}Tc]Tc-HYNIC-CTP was compared to the known myocardial perfusion marker [^{99m}Tc]Tc-Sestamibi in CD1 mice using SPECT/CT imaging.[40] Among the two, [^{99m}Tc]Tc-HYNIC-CTP showed less extra-cardiac uptake than the [^{99m}Tc]Tc-Sestamibi. The administered [^{99m}Tc]Tc-Sestamibi showed cardiac uptake and significant uptake in the liver, gut, and kidneys.[40] On the other hand, [^{99m}Tc]Tc-HYNIC-CTP showed a more targeted heart uptake and no uptake in the liver and gut. There was [^{99m}Tc]Tc-HYNIC-CTP uptake in the heart at early time point post-injection and renal clearance with radioactivity primarily present in the kidneys and bladder.[40] This suggested that [^{99m}Tc]Tc-HYNIC-CTP could be used for cardiac imaging with SPECT. The next logical step was to develop a PET radioisotope labeled CTP probe for PET imaging of cardiac abnormalities. Hence, we synthesized [^{68}Ga]Ga-NOTA-CTP with the PET radionuclide ^{68}Ga and tested its PET imaging potential and *ex vivo* biodistribution in healthy and diseased CD1 mice with myocardial infarction.

Materials and methods

General consideration

All chemicals and solvents were purchased from various commercial manufacturers – Sigma-Aldrich, St Louis, MO, Fisher Scientific, Waltham, MA, and Alfa Aesar, Haverhill, MA and used as received without further purification unless otherwise stated. The NOTA-CTP was custom synthesized by the Peptide & Peptoid Synthesis Facility at the University of Pittsburgh, Pittsburgh, PA, with >97% purity. The mass spectrum, HPLC/UV trace of NOTA-CTP is provided in ESI Fig. S1–S3.† For the radiolabeling, 3.0 M NaOAc (pH 8.4–8.8) buffer was prepared by dissolving 24.6 g of NaOAc in 100 mL of distilled water. Oasis® Millex-GV 0.22 μm (Part No. 186008083) was purchased from Merck, Rahway, NJ. rad-TLC analysis of the reaction mixtures was performed on glass microfiber chromatography paper impregnated with silica gel in 0.1 M sodium citrate solution (pH 5.0) and analyzed using an AR-2000 rad-TLC imaging scanner (Eckert & Ziegler, Valencia, CA). The 0.1 M sodium citrate buffer was prepared by dissolving 0.294 g of sodium citrate dihydrate in 10 mL of distilled water, and the pH was adjusted to 5.0 with 80 μL of concentrated HCl. The final analytical rad-HPLC determined the final purity and identity of compounds performed on a Phenomenex 5 μm, C18(2), 100 Å, LC Column 250 × 4.6 mm (Phenomenex, Torrance, CA),

at a UV detector wavelength of 214 nm. Analytical rad-HPLC was performed using H_2O + 0.1% TFA (solvent A) and CH_3CN + 0.1% TFA (solvent B) with a flow rate of 0.5 mL min^{-1} by applying a gradient method (0–5 min = 24% B to 32.2% B, 5–20 min = 32.2% B to 35% B). [^{68}Ga]Ga-NOTA-CTP was identified between 8.7–9.3 min retention time.

Synthesis of [^{nat}Ga]-NOTA-CTP

To a solution of 150 μg of NOTA-CTP peptide (1.0 μg μL^{-1}) in Milli-Q water, 10 μL of 3 M sodium acetate (NaOAc) buffer was added and pH was adjusted between 4.0 and 4.5 using 1 M HCl. Immediately afterward, 120 μg of $GaCl_3$ solution (12 μg μL^{-1}) was added, and the reaction mixture was incubated at room temperature for 1 hour. UV-HPLC analysis confirmed the formation of [^{nat}Ga]-NOTA-CTP with a 90% yield and a retention time of 8.62 minutes (ESI Fig. S5†).

Radiolabeling

All experiments were performed manually in a sterile hot cell environment. The peptide precursor solution was prepared by dissolving 1.0 mg of the respective peptide (NOTA-CTP) in 1.0 mL distilled water. For the synthesis of [^{68}Ga]Ga-NOTA-CTP, 1.0 mL of [^{68}Ga]$GaCl_3$ (0.2 ± 0.1 GBq) (n = 13) eluted from the ^{68}Ge/^{68}Ga generator (Eckert & Ziegler, Valencia, CA) was transferred into a 5.0 mL reaction vial. The pH of the reaction mixture was adjusted to 4.5–5.0 with 70 μL of 3 M NaOAc (pH 8.4–8.8) before the addition of 150 μg at a concentration of 1.0 μg μL^{-1} of NOTA-CTP solution. Then, the reaction mixture was allowed to stir for up to 10 min at RT. The radiolabeling yield was analyzed by rad-TLC using 0.1 M sodium citrate solution (pH 5.0) as the mobile phase. The final pH of the reaction mixture was adjusted to 6.1–6.5 with an additional 170 μL of 3 M NaOAc (pH 8.4–8.8) and passed through a Millex-GV 0.22 μm sterile filter unit. If the radiochemical purity calculated by rad-HPLC was less than 96%, the reaction mixture was purified from a reverse phase rad-HPLC, and final product was concentrated using a C-18 SepPak cartridge and eluted with a solution of 25% EtOH in NaOAc (1 M) followed by addition of a saline solution (0.9%) reaching a final formulation of 10/30/60 v/v/v ethanol/1.0 M sodium acetate/saline. [^{68}Ga]Ga-NOTA-CTP was obtained in 68.9 ± 12.8 (n = 13) decay corrected radiochemical yield, 1.3 ± 0.5 GBq per μmol (n = 13) of molar activity (Am) and >97.8% radiochemical purity after HPLC semipreparative purification confirmed by analytical rad-HPLC at the end of the synthesis (ESI Fig. S4†). Total synthesis and formulation time was 30 min without purification and 60 min with HPLC purification from when [^{68}Ga]$GaCl_3$ was transferred into the reaction vial. The radiochemical purity of the synthesized [^{68}Ga]Ga-NOTA-CTP was analyzed by analytical rad-HPLC having a retention time of 8.76 min (ESI Fig. S4†). Molar activity (Am) was measured by dividing the radioactivity (GBq) present at the end of the synthesis with the amount of NOTA-CTP (μmol) present in the final formulation.

Stability analysis

The stability of [^{68}Ga]Ga-NOTA-CTP was assessed in the final formulation (10/30/60 v/v/v ethanol/1.0 M sodium acetate/saline) incubated at room temperature up to 120 min with 20 min intervals using analytical rad-HPLC. The stability in human and mouse sera was assessed by rad-TLC using 0.1 M Sodium citrate buffer (pH = 5.0) as a mobile phase at 0 min, 30 min, 60 min, and 120 min post-incubation. For the serum stability studies, 100 μL of [^{68}Ga]Ga-NOTA-CTP (~37.0 MBq) was added to 100 μL of human serum or mouse serum in an Eppendorf tube. The mixture was then incubated at 37 °C and stirred at 1500 rpm in a thermomixer for up to 120 min. A small aliquot (~0.5 μL) was taken out at different time points for rad-TLC.

Animals

Healthy CD1 mice (n = 9, body weight 35.45 ± 6.54 g) and CD1 mice with myocardial infarction (n = 7, body weight 31.35 ± 6.32 g) were obtained from Envigo RMS LLC, Indianapolis, IN. These animals were received and housed at the Department of Comparative Medicine facility at the Mayo Clinic, Rochester, MN. Table 1 shows the age and sex of mice used in the study. The myocardial infarction was induced by the ligation of the left anterior descending artery following thoracotomy under surgical anesthesia, leading to ischemia of the anterior and anteroseptal myocardium at Envigo RMS LLC, Indianapolis, IN. Postoperative care was provided for 3 days at Envigo RMS LLC, Indianapolis, IN, to mitigate the complications associated with infarction and anesthesia before being shipped to Mayo Clinic Rochester. At Mayo Clinic, the animals were nourished with a regular diet and water *ad libitum* and were maintained at optimal conditions of 40% relative humidity and 22 °C temperature with 12-hour light–dark cycles.

PET/CT imaging

Animals were injected with 2.29 ± 0.83 MBq (62.00 ± 22.31 μCi) of [^{68}Ga]Ga-NOTA-CTP (n = 16) through the tail vein under 1–2.5% isoflurane anesthesia. Animals underwent whole-body dynamic PET-CT using a small animal microPET/CT imaging system, Inveon (Siemens Medical Solutions USA, Malvern, PA), immediately after injection for 30 min with a framing sequence of 4 × 15 s, 8 × 30 s, 5 × 60 s, 4 × 300 s. A CT scan for 7 minutes followed each PET scan. The PET/CT images were reconstructed using Siemens Inveon Micro PET-CT proprietary software. For analysis of PET/CT images, the PET and CT images were overlayed using MIM-7.2.7 software (MIM Software Inc., Cleveland, OH). ROIs were drawn in the heart in the overlayed CT images to delineate the whole heart, left atrium (LA), right atrium (RA), left ventricle (LV), and right ventricle (RV), as shown in ESI Fig. S6.† The mean concentration of the PET signal was quantified in the overlayed PET image in kBq per cc in the ROI for whole heart, left and right ventricle, which was converted to μCi per cc. The SUV was calculated using decay-corrected activity values in the following formula:

$$SUV_{ROI} = \frac{\text{mean concentration (}\mu\text{Ci per g or }\mu\text{Ci per cc)in ROI}}{\text{injected dose (}\mu\text{Ci)}} \times \text{weight of animal (g or cc)}$$

Table 1 Age and sex of mice used during the study

Healthy CD1 mice (n = 9)	Age (week) average ± SD	Body weight (g) average ± SD
Males (n = 5)	10.69 ± 2.44	39.80 ± 4.27
Females (n = 4)	10.36 ± 2.69	30.03 ± 4.36
CD1 mice with myocardial infarction (n = 8)	**Age (week) average ± SD**	**Body weight (g) average ± SD**
Males (n = 4)	9.79 ± 1.74	35.24 ± 5.54
Females (n = 4)	8.96 ± 1.75	27.03 ± 2.24

Ex vivo biodistribution

The animals were transferred to a heating pad under a 1–2.5% isoflurane maintenance dose after the final imaging scan. A midline incision was made, and all the organs were harvested, including the heart. The heart was then placed on a Petri dish and perfused with 10.0 mL of phosphate-buffered saline (PBS) using a 10 mL syringe through the left ventricular apex, clearing the blood in all the chambers. The dissected organs were transferred to labeled and preweighed vials and counted in 2480 Wizard 2 automatic gamma counter (PerkinElmer, Waltham, MA) for decay-corrected ^{68}Ga counts. SUV was then calculated using the following formula:

$$\mathrm{SUV_{tissue}} = \frac{^{68}\mathrm{Ga\ concentration\left(counts\ per\ g_{tissue}\right)}}{\mathrm{injected\ dose\ (counts)}} \times \mathrm{weight\ of\ animal\ (g)}$$

Statistical analysis

The uptake data was analyzed using the Excel spreadsheet program (Microsoft Corporation, Redmond, WA). Uptake was compared multifold between different heart regions and other major organs using unpaired Student t-test analysis. P-Values less than 0.05 were considered statistically significant.

Ethical standards

All animal studies were performed after approval and under the Mayo Clinic's Institutional Animal Care and Use Committee (IACUC) guidelines and regulations.

Results and discussion

Chemistry

The NOTA-CTP was custom synthesized at the Peptide & Peptoid Synthesis Facility at the University of Pittsburgh, Pittsburgh, PA, with >97% purity (ESI Fig. S1–S3†).

Radiochemistry

^{68}Ga-labeling of NOTA-CTP was performed following our previous standardized protocol[52] for radiolabeling peptides (Fig. 1). [^{68}Ga]GaCl$_3$ obtained from a ^{68}Ge/^{68}Ga generator was used for the radiolabeling. The labeling was carried out at pH 4.5–5.0 with 150 μg of precursor (optimized concentration, Table 2) by incubating for up to 10 min at room temperature (RT). Radiolabeling yield was confirmed by rad-TLC using 0.1 M sodium citrate solution at pH 5.0 as the mobile phase (ESI Fig. S7†). [^{68}Ga]Ga-NOTA-CTP was obtained with a decay-corrected radiochemical yield of 68.9 ± 12.8% (n = 13) and molar activity (Am) of 1.3 ± 0.5 GBq per μmol (n = 13) with >97.8% radiochemical purity, calculated by rad-HPLC, after HPLC semipreparative purification at the end of the synthesis (ESI Fig. S4†).

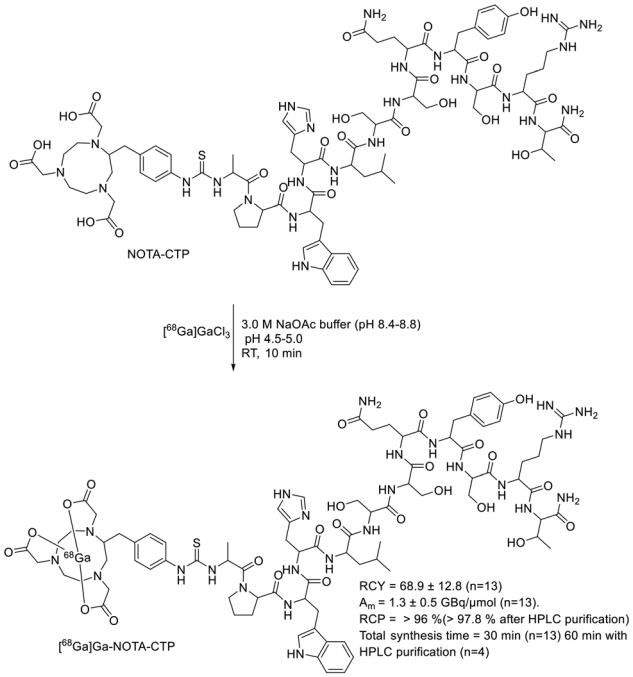

Fig. 1 Radiosynthesis of [^{68}Ga]Ga-NOTA-CTP.

Table 2 Optimization of CTP concentration for synthesis of [^{68}Ga]Ga-NOTA-CTP

S. No	Concentration of NOTA-CTP (μg mL^{-1})	Reaction time (min)	Reaction conversion (%) based on rad-TLC
1	69.57	10	76.00[a]
2	69.57	20	81.00[a]
3	69.57	30	87.00[a]
4	100.84	10	98.00[a]
5	122.95	10	100.00[a]

Reaction conditions: pH 4.5–5.0, 70 μL of 3 M NaOAc (pH 8.4–8.8), RT.
[a] Reaction conversion was measured by rad-TLC.

Stability assessment in formulation and serum

The radiochemical purity of [^{68}Ga]Ga-NOTA-CTP decreased from 98.78 ± 1.08% (n = 4) at 0 min post-synthesis to 92.52 ± 3.66% (n = 4) at 2 h post-synthesis in the formulation (Fig. 2A and ESI Table S1†). Although we saw decreased radiochemical purity by rad-HPLC based on [^{68}Ga]Ga-NOTA-CTP peak, we did not observe free ^{68}Ga leaching from the molecule up to 120 min in the rad-HPLC chromatogram at the retention time of ~3.35 min (ESI Fig. S7 and S8†). Thus, the impurities contributing to decreased radiochemical purity resulted from the peptide degradation, likely forming labeled fragments with a lower Rf and not related to the stability of the ^{68}Ga-radiolabeling.

The stability of [^{68}Ga]Ga-NOTA-CTP was assessed in human and mouse sera incubated at 37 °C in a thermomixer with 1500 rpm for up to 120 min by rad-TLC at 0 min, 30 min, 60 min, and 120 min post-incubation. The results are summarized in Fig. 2B, and representative chromatograms are presented in ESI Fig. S9 and S10,† followed by the tabulated values in ESI Table S2.† Interestingly, [^{68}Ga]Ga-NOTA-CTP maintained stability above 96.33 ± 1.96% in mouse serum (n = 5) and 97.96 ± 0.37% in human serum (n = 4) during the first hour of incubation, with its stability decreasing to 93.55 ± 1.62% in mouse serum (n = 5) and 93.98 ± 0.98% in human serum (n = 4) after 2 hours of incubation at 37 °C. Although it seems [^{68}Ga]Ga-NOTA-CTP was more stable in human serum than in formulation, but it should be noted that stability in formulation was assessed by rad-HPLC and stability in serum was assessed by rad-TLC. The rad-TLC does not have sufficient resolution to identify peptide degradation. It is likely that the labeling is equally stable in formulation and sera with similar peptide degradation but was not visible on the rad-TLC. Considering the lower amount of radioactivity (~185 MBq) used as ^{68}Ga for the synthesis of [^{68}Ga]-NOTA-CTP, this study does not assess any potential radiolysis during large scale (high radioactivity) clinical production of [^{68}Ga]-NOTA-CTP.

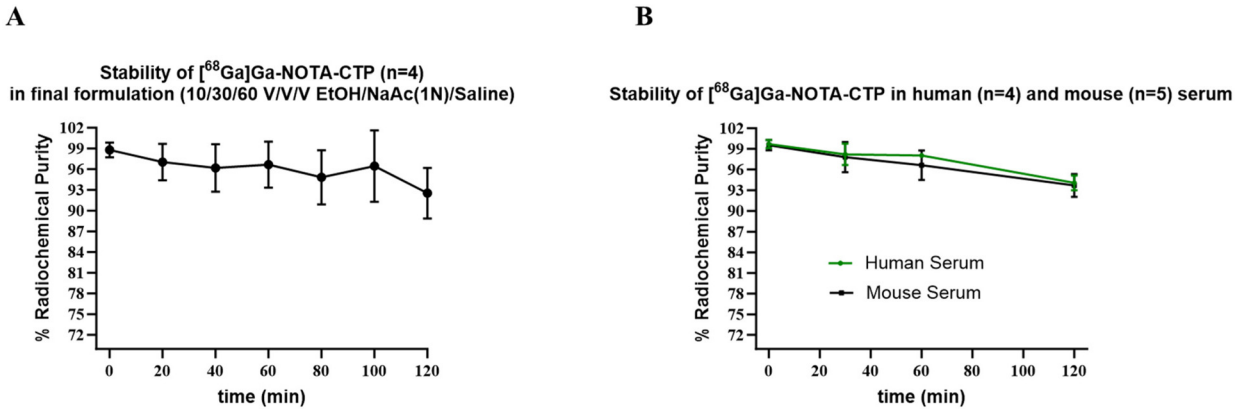

Fig. 2 [^{68}Ga]Ga-NOTA-CTP stability over time. (A) Stability of the radiotracer in the formulation up to 120 min (n = 4), (B) stability of the radiotracer up to 120 min in human (n = 4) and mouse (n = 5) sera.

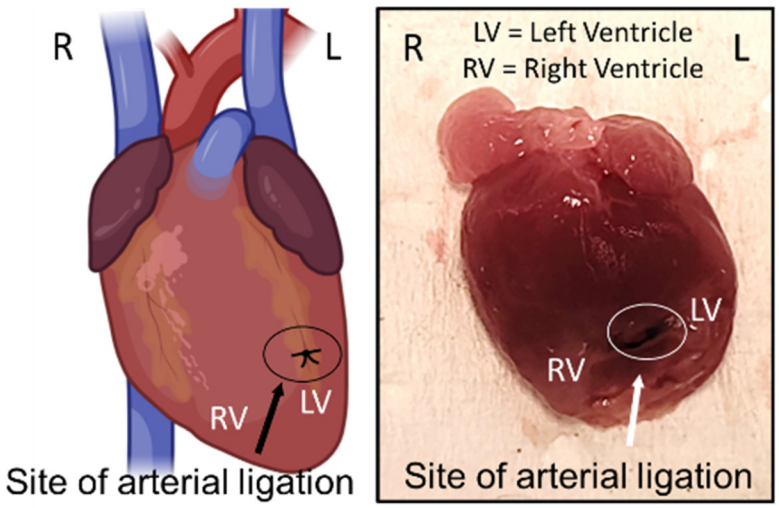

Fig. 3 Schematic diagram showing ligation site in the left anterior descending artery of an infarcted heart.

Table 3 Biodistribution of [^{68}Ga]Ga-NOTA-CTP in healthy CD1 mice assessed by PET imaging

Timepoint (min)	SUV heart (average ± SD, n = 9)	SUV liver (average ± SD, n = 9)	SUV muscle (average ± SD, n = 9)	SUV kidneys (average ± SD, n = 9)	SUV urinary bladder (average ± SD, n = 9)
0–5	0.91 ± 0.15	1.42 ± 0.49	0.36 ± 0.12	2.64 ± 0.89	7.51 ± 3.49
6–10	0.59 ± 0.09	1.66 ± 0.58	0.28 ± 0.15	2.15 ± 1.21	10.73 ± 5.16
11–20	0.46 ± 0.08	1.79 ± 0.55	0.25 ± 0.15	1.91 ± 1.29	12.46 ± 5.86
21–30	0.33 ± 0.07	1.83 ± 0.54	0.21 ± 0.16	1.71 ± 1.37	14.31 ± 6.88
60	0.04 ± 0.04 (n = 6)	0.69 ± 0.32 (n = 3)	0.18 ± 0.13 (n = 7)	0.92 ± 0.68 (n = 3)	10.64 ± 6.10
120	0.02 ± 0.01 (n = 6)	0.14 (n = 1)	0.19 ± 0.18 (n = 5)	0.1 (n = 1)	9.02 ± 8.59 (n = 6)

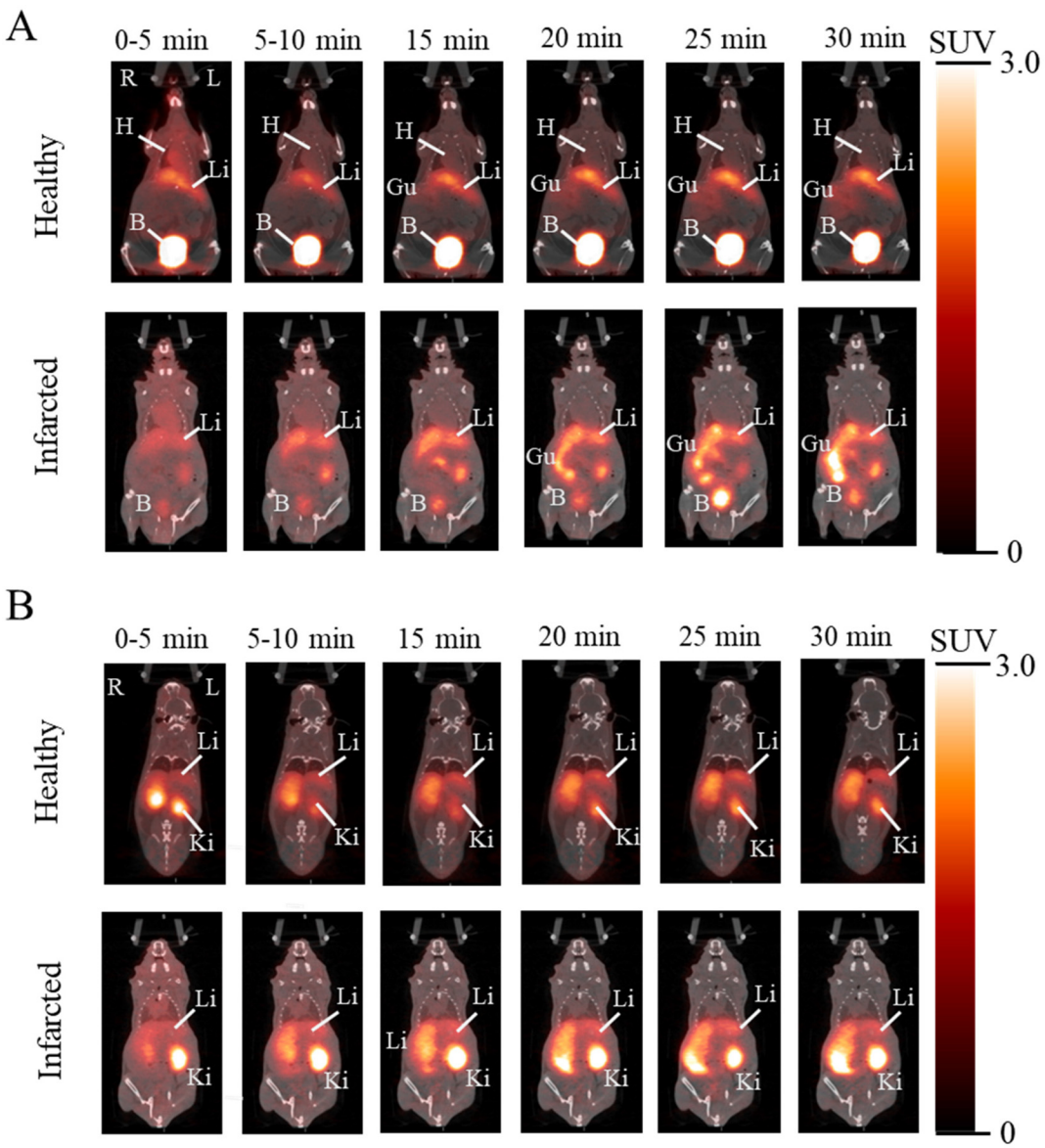

Fig. 4 Representative coronal PET/CT image showing [^{68}Ga]Ga-NOTA-CTP uptake in heart, liver, gut, kidneys, gall bladder, and bladder of healthy and infarcted CD1 mice at different time points post-injection. The PET/CT images are presented in two different planes, A and B, to visualize different organs in various planes. In each plane, the top row shows a healthy mouse, and the bottom row shows an infarcted mouse. H = Heart, Li = Liver, Ki = Kidney and Gu = Gut.

Imaging and biodistribution

Based on the stability profile, the developed radiotracer showed sufficient stability and purity (>98% by rad-TLC) at the time of animal injection.

In cardiac studies, the use of larger species, such as canine or porcine ligation models, offers physiology and behavior like humans. However, the disadvantages of larger species include the high cost, the need for dedicated facilities for these species, and an increase in the complexity of handling. According to the International Atomic Energy Agency's recommendations for the preclinical development of radiopharmaceuticals, the use of small animals such as mice and rats has several advantages over large animals.[53] The advantages include the possibility of performing whole-body dynamic studies in conventional micro imaging equipment, low cost and easy handling. The infarct model used in this study is well established in mice and commercially available. Our laboratory has a micro-PET scanner (used for this work) that allows us to obtain PET images in mice, which was one of the reasons for selecting the murine model.

The biodistribution of [^{68}Ga]Ga-NOTA-CTP was assessed by PET/CT imaging at several time points post-injection in

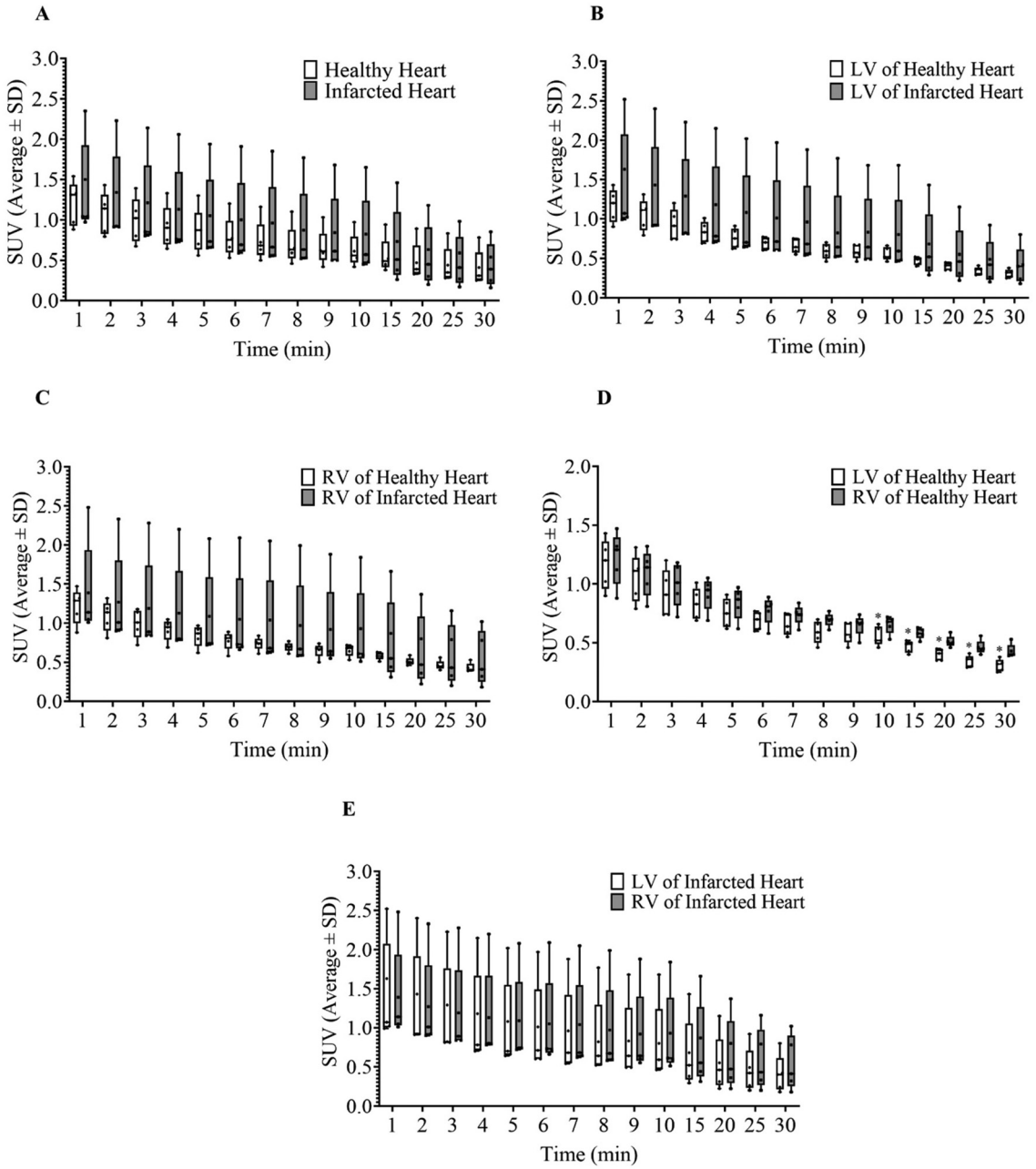

Fig. 5 Uptake of [^{68}Ga]Ga-NOTA-CTP in healthy and infarcted hearts, (A) uptake in whole heart and (B–E) uptake in ventricles of healthy and infarcted hearts of CD1 mice, assessed by PET/CT imaging. LV = left ventricle and RV = right ventricle. *P value < 0.05 LV *vs.* RV in healthy heart.

healthy and diseased CD1 mice with myocardial infarction. In this diseased model, infarction was induced in the heart of CD1 mice by ligating the left anterior descending artery (Fig. 3). Following ligation, the mice were allowed to recuperate for up to 6 weeks with intact ligation in the heart, mimicking chronic myocardial infarction. Prior studies evaluated cardiac changes during the first 8 weeks post ligation of the left anterior descending artery and observed increase in the end-diastolic volume (EDV) and end-systolic volume (ESV) and decrease in the ejection fraction compared to a healthy heart.[54–56] This is because the ligation causes rerouting of blood supply with regional decreased to absent perfusion with subsequent cardiac remodeling.[54–56] An imaging tracer that could detect these changes at the initial stages would allow the identification of subjects at risk for adverse remodeling, leading to early interventions. Therefore, in our study, [^{68}Ga]Ga-NOTA-CTP was administered within 6 weeks of the surgery, and its distribution was assessed and compared with healthy animals.

Generally, the administered peptides are primarily cleared from the blood through renal clearance without reabsorption, leading to high urinary bladder activity.[57] Serial PET/CT imaging of the healthy animals post-administration of [^{68}Ga]Ga-NOTA-CTP showed that the biodistribution profile of [^{68}Ga]Ga-NOTA-CTP was typical for peptides. The administered [^{68}Ga]Ga-NOTA-CTP had high bladder activity as early as 0–5 min post-injection, with continued urinary clearance until 120 min post-injection (Table 3 and Fig. 4). The major organs taking up [^{68}Ga]Ga-NOTA-CTP were the urinary bladder, kidneys, heart, and liver until 30 min post-injection (Table 3). No or low signal was detected in the heart, kidneys, and liver at 60 min and 120 min post-injection, with the majority of signal present in the urinary bladder (Table 3).

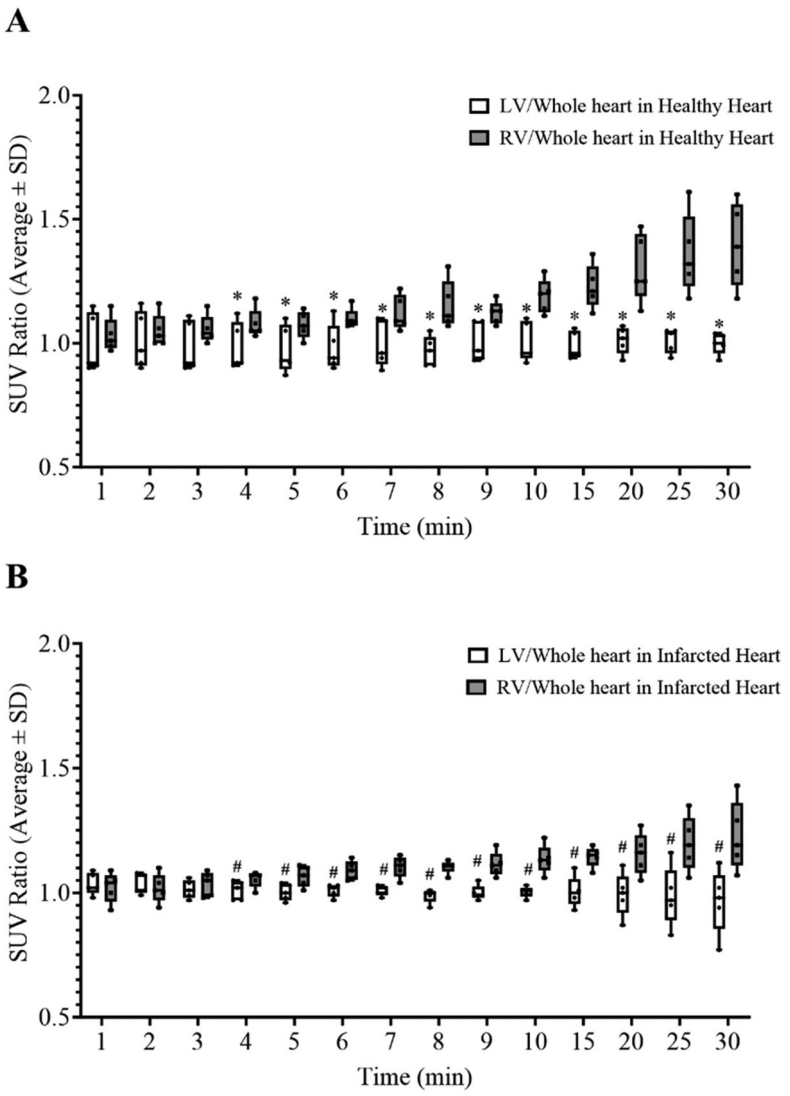

Fig. 6 Uptake of [^{68}Ga]Ga-NOTA-CTP in left and right ventricles normalized to whole heart, (A) healthy heart and (B) infarcted heart of CD1 mice, assessed by PET/CT imaging. LV/H = left ventricle/whole heart and RV/H = right ventricle/whole heart. *P value < 0.05 LV/H *vs.* RV/H in healthy heart; #P value < 0.05 LV/H *vs.* RV/H in infarcted heart.

An ideal cardiac perfusion marker should show high initial uptake in the heart and rapid clearance from the blood pool.[58] Indicative of being a promising perfusion marker, we observed a high uptake of [^{68}Ga]Ga-NOTA-CTP (SUV > 1) in the healthy heart immediately after the intravenous administration, followed by a rapid clearance within 30 min of administration (Table 3 and Fig. 5, ESI Table S3A†). Noticing a faster clearance, [^{68}Ga]Ga-NOTA-CTP uptake was evaluated more closely within 30 min post-injection at several time points (Fig. 5 and 6, ESI Tables S3A and S3B†). The CT images were used to draw regions of interest in the whole heart, left, and right ventricles to assess the uptake of [^{68}Ga]Ga-NOTA-CTP in these regions in the PET scans (Fig. 4 and ESI Fig. S6†).

Regarding the whole heart uptake of [^{68}Ga]Ga-NOTA-CTP, we observed no statistical difference in the uptake in the infarcted heart as compared to the healthy heart at all time points within 30 min post-injection (Fig. 5 and ESI Table S3A†). An infarcted heart is known to undergo remodeling and rerouting of blood supply that could impact uptake of perfusion markers.[54–56] Regional differences in [^{68}Ga]Ga-NOTA-CTP uptake in the left ventricle (LV) or right ventricle (RV) in the whole heart (WH) in healthy and infarcted animals were compared (Fig. 5 and 6, and ESI Tables S3A and S3B†). Within a healthy heart, the SUV in LV was lower than the RV at the 10–30 min post-injection time point (Fig. 5 and ESI Table S3A†). This difference between uptake in LV and RV was absent in the infarcted heart (Fig. 5 and ESI Table S3A†). It is possible that dilation of LV and increased EDV in the infarcted heart contributed to higher retention of [^{68}Ga]Ga-NOTA-CTP in LV in the infarcted heart.[54–56,59] Additionally, we also compared the ratio of uptake in LV and RV normalized to the entire heart (Fig. 6 and ESI Table S3B†). In both infarcted and healthy hearts, the LV/whole heart SUV ratio was lower than the RV/whole heart SUV ratio at 4–30 min post-injection time point (Fig. 6 and ESI Table S3B†).

In the context of adverse remodeling, after the acute phase of an infarction, the heart undergoes a process of scarring and remodeling, which leads to changes in its geometry, dimensions, and function.[60] Adverse remodeling of the left ventricle involves molecular, cellular, and interstitial changes within the tissue.[61] This process often occurs following an ST-Segment Elevation Myocardial Infarction (STEMI), which results from the blockage of one or more coronary arteries.[61] In such cases, a scarred area typically forms, and the patient may develop HF with either a reduced or mildly reduced ejection fraction (EF). EF is a key measure of the heart's ability to pump blood out the left ventricle. In our experiments, we observed a trend of higher uptake of the radiotracer in the left ventricle of the infarcted model compared to the healthy group (Fig. 5). This observed increase in blood retention of [^{68}Ga]Ga-NOTA-CTP in the infarcted left ventricle implies a lower ejection fraction and potential adverse remodeling of the left ventricle in the infarcted model.

The animals with infarcted hearts showed biodistribution profiles in all organs/tissues similar to healthy animals at 120 min post-injection, as assessed by *ex vivo* biodistribution except the heart (Table 4). Overall, the uptake of [^{68}Ga]Ga-NOTA-CTP was low in heart; however, the infarcted heart showed statistically higher uptake of [^{68}Ga]Ga-NOTA-CTP (SUV = 0.03 ± 0.02, n = 7) as compared to the healthy heart (SUV = 0.02 ± 0.006, n = 9). Most of the radioactivity was found in organs involved in excretion, like the gallbladder, urinary bladder, small intestine, and cecum at 120 min post injection (Table 4). High urinary and gallbladder uptake also confirmed renal and hepatobiliary excretion of [^{68}Ga]Ga-NOTA-CTP (Table 4).

In an earlier study, [^{68}Ga]Ga-DOTA was tested as a cardiac perfusion marker at 24 ± 4 h post-coronary ligation.[59] In this myocardial infarction rat model, higher uptake of [^{68}Ga]Ga-DOTA was observed at the infarct site compared to a remote site within the heart at 30 min post-administration of [^{68}Ga]Ga-DOTA.[59] This suggests that remodeling and rerouting of the heart's blood supply could be underway as early as 24 ± 4 h, contributing to delayed washout and increased retention of [^{68}Ga]Ga-DOTA at the infarct site aligning with our findings.[59] Additionally, in the present study [^{68}Ga]Ga-NOTA-CTP was assessed in the chronically infarcted heart model but there were previous studies where other radiotracers were assessed in acutely infarcted heart model. In an acutely infarcted heart model, the ligation of the left anterior descending coronary artery has occurred within 3–24 h of imaging. Hence, the heart is still in shock with severe perfusion changes.[62–65] Perfusion markers can demonstrate profound changes in cardiac perfusion in the acute infarction model. There are many preclinical studies done with acute infarction heart rodent models showing decreased perfusion utilizing [^{99m}Tc]Tc-MIBI, ^{13}N-ammonia, [^{18}F]F-flurpiridaz, and ^{82}Rb at the infarct site.[62–65] The chronically infarcted heart rodent models use

Table 4 *Ex vivo* biodistribution of [^{68}Ga]Ga-NOTA-CTP in healthy and infarcted CD1 mice at 120 min post-injection

Organ	Healthy mice SUV (average ± SD, n = 9)	Infarcted mice SUV (average ± SD, n = 7)
Brain	0.01 ± 0.004	0.005 ± 0.003
Heart	0.02 ± 0.006	0.03 ± 0.02*
Lung	0.04 ± 0.02	0.04 ± 0.04
Liver	0.22 ± 0.16	0.15 ± 0.04
Kidneys	0.85 ± 0.28	0.63 ± 0.21
Spleen	0.04 ± 0.03	0.05 ± 0.04
Small intestine	2.74 ± 1.29	3.38 ± 2.37
Large intestine	0.94 ± 1.30	1.21 ± 1.26
Pancreas	0.05 ± 0.06	0.05 ± 0.04
Muscle	0.03 ± 0.03	0.02 ± 0.01
Urine	52.68 ± 27.34	39.68 ± 37.93
Bone	0.83 ± 2.35	0.03 ± 0.02
Bladder	5.11 ± 5.63	6.53 ± 13.43
Skin	0.02 ± 0.01	0.03 ± 0.03
Adipose	0.06 ± 0.08	0.05 ± 0.05
Stomach	0.06 ± 0.07	0.08 ± 0.10
Cecum	2.36 ± 2.24	2.28 ± 3.64
Blood	0.05 ± 0.05	0.02 ± 0.01
Feces	5.43 ± 8.97	7.00 ± 7.72
Gall bladder	23.48 ± 19.28 (n = 5)	12.17 ± 13.13 (n = 3)

*P value < 0.05 healthy mice *vs.* infarcted mice

[^{18}F]FDG to assess other parameters such as left ventricular metabolic volume (LVMV), defect/infarct area, and cardiac function.[63,64] The infarction model used in this study was generated by Envigo RMS LLC, Indianapolis, IN, followed by a 3-day observation period at their site. Therefore, testing [^{68}Ga]Ga-NOTA-CTP within ~24 hours post-surgery was impossible. We did not find PET imaging-based perfusion marker studies in a chronically infarcted heart rodent model. Therefore, this opportunity to assess if [^{68}Ga]Ga-NOTA-CTP can detect perfusion differences in a remodeled chronically infarcted heart was reasonable and informative.

Conclusions

After administration, the radiolabeled cardiac targeting peptide, [^{68}Ga]Ga-NOTA-CTP, was rapidly cleared from the body *via* the renal and hepatobiliary routes. The uptake of [^{68}Ga]Ga-NOTA-CTP in the whole heart was similar in chronically infarcted and healthy hearts, but [^{68}Ga]Ga-NOTA-CTP could identify regional differences in the left ventricular *vs.* right ventricular uptake between the healthy and diseased hearts. This ability to detect regional differences indicates the potential of [^{68}Ga]Ga-NOTA-CTP as a perfusion marker.

Safety and hazards

This study includes use of radioactive materials. Proper institutional guidelines and precautions should be taken while working with radioactive materials.

Author contributions

S.R.G.: investigation, validation, curation, and analysis of data, and writing the manuscript. M.K.: investigation, validation, curation, and analysis of data, and writing the manuscript. A. G.R.: investigation, validation, curation, and analysis of data, and writing the manuscript. A.B.: investigation, validation, curation, and analysis of data, and writing the manuscript. V. K.: investigation, validation, curation, and analysis of data, and writing the manuscript. D.A.S.: animal ordering, reviewing, and editing the manuscript. J.E.K.: reviewing and editing the manuscript. D.R.J.: reviewing and editing the manuscript. M.Z.: resources, reviewing and editing the manuscript. V.J.L.: resources, reviewing and editing the manuscript. M.K.P.: conceptualization, fund acquisition, methodology, project administration, resources, supervision, software, and writing, reviewing, and editing the manuscript.

Data availability

The entire data generated and analyzed during this study are included in the main manuscript and its ESI.†

Conflicts of interest

All the authors declare no competing conflict of interest. M.Z. is the inventor of CTP.

Acknowledgements

This study was funded by the Department of Radiology and Department of Cardiovascular Medicine, Mayo Clinic, Rochester, MN USA. MZ is supported by an R01 grant HL153407 from NHLBI.

References

1 J. P. Duggan, A. S. Peters, G. D. Trachiotis and J. L. Antevil, *Surg. Clin. North. Am.*, 2022, **102**, 499–516.
2 K. Wang, X. Shi, Z. Zhu, X. Hao, L. Chen, S. Cheng, R. S. Y. Foo and C. Wang, *Genome Med.*, 2022, **14**, 63.
3 J. S. Lawton, J. E. Tamis-Holland, S. Bangalore, E. R. Bates, T. M. Beckie, J. M. Bischoff, J. A. Bittl, M. G. Cohen, J. M. DiMaio, C. W. Don, S. E. Fremes, M. F. Gaudino, Z. D. Goldberger, M. C. Grant, J. B. Jaswal, P. A. Kurlansky, R. Mehran, T. S. Metkus, Jr., L. C. Nnacheta, S. V. Rao, F. W. Sellke, G. Sharma, C. M. Yong and B. A. Zwischenberger, *Circulation*, 2022, **145**, e4–e17.
4 S. S. Virani, A. Alonso, H. J. Aparicio, E. J. Benjamin, M. S. Bittencourt, C. W. Callaway, A. P. Carson, A. M. Chamberlain, S. Cheng, F. N. Delling, M. S. V. Elkind, K. R. Evenson, J. F. Ferguson, D. K. Gupta, S. S. Khan, B. M. Kissela, K. L. Knutson, C. D. Lee, T. T. Lewis, J. Liu, M. S. Loop, P. L. Lutsey, J. Ma, J. Mackey, S. S. Martin, D. B. Matchar, M. E. Mussolino, S. D. Navaneethan, A. M. Perak, G. A. Roth, Z. Samad, G. M. Satou, E. B. Schroeder, S. H. Shah, C. M. Shay, A. Stokes, L. B. VanWagner, N. Y. Wang and C. W. Tsao, *Circulation*, 2021, **143**, e254–e743.
5 G. A. Roth, G. A. Mensah, C. O. Johnson, G. Addolorato, E. Ammirati, L. M. Baddour, N. C. Barengo, A. Z. Beaton, E. J. Benjamin, C. P. Benziger, A. Bonny, M. Brauer, M. Brodmann, T. J. Cahill, J. Carapetis, A. L. Catapano, S. S. Chugh, L. T. Cooper, J. Coresh, M. Criqui, N. DeCleene, K. A. Eagle, S. Emmons-Bell, V. L. Feigin, J. Fernández-Solà, G. Fowkes, E. Gakidou, S. M. Grundy, F. J. He, G. Howard, F. Hu, L. Inker, G. Karthikeyan, N. Kassebaum, W. Koroshetz, C. Lavie, D. Lloyd-Jones, H. S. Lu, A. Mirijello, A. M. Temesgen, A. Mokdad, A. E. Moran, P. Muntner, J. Narula, B. Neal, M. Ntsekhe, G. Moraes de Oliveira, C. Otto, M. Owolabi, M. Pratt, S. Rajagopalan, M. Reitsma, A. L. P. Ribeiro, N. Rigotti, A. Rodgers, C. Sable, S. Shakil, K. Sliwa-Hahnle, B. Stark, J. Sundström, P. Timpel, I. M. Tleyjeh, M. Valgimigli, T. Vos, P. K. Whelton, M. Yacoub, L. Zuhlke, C. Murray and V. Fuster, *J. Am. Coll. Cardiol.*, 2020, **76**, 2982–3021.
6 S. T. Dahlberg, *J. Nucl. Cardiol.*, 2009, **16**, 493–496.

7 O. O. Sogbein, M. Pelletier-Galarneau, T. H. Schindler, L. Wei, R. G. Wells and T. D. Ruddy, *BioMed Res. Int.*, 2014, **2014**, 942960.
8 R. Mikołajczak and P. Garnuszek, *Nucl. Med. Rev. Cent. East. Eur.*, 2012, **15**, 39–45.
9 D.-Y. Kim, H.-J. Kim, K.-H. Yu and J.-J. Min, *Bioconjugate Chem.*, 2012, **23**, 431–437.
10 V. Sharma, J. Sivapackiam, S. E. Harpstrite, J. L. Prior, H. Gu, N. P. Rath and D. Piwnica-Worms, *PLoS One*, 2014, **9**, e109361.
11 A. Y. Ji, Q. M. Jin, D. J. Zhang, H. Zhu, C. Su, X. H. Duan, L. Bian, Z. P. Sun, Y. C. Ni, J. Zhang, Z. Yang and Z. Q. Yin, *ACS Med. Chem. Lett.*, 2017, **8**, 191–195.
12 M. K. Pandey, A. P. Belanger, S. Wang and T. R. DeGrado, *J. Med. Chem.*, 2012, **55**, 10674–10684.
13 T. R. DeGrado, M. K. Pandey, A. P. Belanger, F. Basuli, A. Bansal and S. Wang, *Am. J. Physiol. Endocrinol. Metab.*, 2019, **316**, E251–E259.
14 T. R. DeGrado, F. Bhattacharyya, M. K. Pandey, A. P. Belanger and S. Wang, *J. Nucl. Med.*, 2010, **51**, 1310–1317.
15 M. Dietz, C. H. Kamani, V. Dunet, S. Fournier, V. Rubimbura, N. Testart Dardel, A. Schaefer, M. Jreige, S. Boughdad, M. Nicod Lalonde, N. Schaefer, N. Mewton, J. O. Prior and G. Treglia, *Front. Med.*, 2022, **9**, 887508.
16 M. K. Pandey, F. Bhattacharyya, A. P. Belanger, S. Wang and T. R. DeGrado, *Circulation*, 2010, **122**, A12657–A12657.
17 T. M. Bateman, *J. Nucl. Cardiol.*, 2012, **19**(Suppl 1), S3–11.
18 R. S. Driessen, P. G. Raijmakers, W. J. Stuijfzand and P. Knaapen, *Int. J. Cardiovasc. Imaging*, 2017, **33**, 1021–1031.
19 I. Carvajal-Juarez, A. Monroy-Gonzalez, N. Espinola-Zavaleta, A. Meave-Gonzalez and E. Alexanderson-Rosas, *Ann. Nucl. Cardiol.*, 2019, **5**, 63–68.
20 H. R. Schelbert, M. E. Phelps, S. C. Huang, N. S. MacDonald, H. Hansen, C. Selin and D. E. Kuhl, *Circulation*, 1981, **63**, 1259–1272.
21 J. Maddahi and R. R. Packard, *Semin. Nucl. Med.*, 2014, **44**, 333–343.
22 M. F. Di Carli, S. Dorbala, J. Meserve, G. El Fakhri, A. Sitek and S. C. Moore, *J. Nucl. Med.*, 2007, **48**, 783–793.
23 S. Senthamizhchelvan, P. E. Bravo, C. Esaias, M. A. Lodge, J. Merrill, R. F. Hobbs, G. Sgouros and F. M. Bengel, *J. Nucl. Med.*, 2010, **51**, 1592–1599.
24 P. Arumugam, D. Tout and C. Tonge, *Br. Med. Bull.*, 2013, **107**, 87–100.
25 H. A. Ziessman, J. P. O'Malley, J. H. Thrall and F. H. Fahey, in *Nuclear Medicine (Fourth Edition)*, ed. H. A. Ziessman, J. P. O'Malley and J. H. Thrall, W.B. Saunders, Philadelphia, 2014, p. ix, DOI: **10.1016/B978-0-323-08299-0.05001-X**.
26 H. Iida, I. Kanno, A. Takahashi, S. Miura, M. Murakami, K. Takahashi, Y. Ono, F. Shishido, A. Inugami, N. Tomura and, *et al.*, *Circulation*, 1988, **78**, 104–115.
27 C. C. Yang, *Diagnostics*, 2021, **11**, 2275.
28 J. T. Thackeray, J. P. Bankstahl, Y. Wang, M. Korf-Klingebiel, A. Walte, A. Wittneben, K. C. Wollert and F. M. Bengel, *Eur. J. Nucl. Med. Mol. Imaging*, 2015, **42**, 317–327.
29 E. A. McCutchan, *Nucl. Data Sheets*, 2012, **113**, 1735–1870.
30 M. K. Pandey, J. F. Byrne, H. Jiang, A. B. Packard and T. R. DeGrado, *Am. J. Nucl. Med. Mol. Imaging*, 2014, **4**, 303–310.
31 H. M. Sherif, A. Saraste, E. Weidl, A. W. Weber, T. Higuchi, S. Reder, T. Poethko, G. Henriksen, D. Casebier, S. Robinson, H. J. Wester, S. G. Nekolla and M. Schwaiger, *Circ. Cardiovasc. Imaging*, 2009, **2**, 77–84.
32 J. Maddahi, J. Czernin, J. Lazewatsky, S. C. Huang, M. Dahlbom, H. Schelbert, R. Sparks, A. Ehlgen, P. Crane, Q. Zhu, M. Devine and M. Phelps, *J. Nucl. Med.*, 2011, **52**, 1490–1498.
33 N. Matsumoto, *Ann. Nucl. Cardiol.*, 2023, **9**, 91–93.
34 R. C. Marshall, P. Powers-Risius, B. W. Reutter, J. P. O'Neil, M. La Belle, R. H. Huesman and H. F. VanBrocklin, *J. Nucl. Med.*, 2004, **45**, 1950–1959.
35 I. Madar, H. T. Ravert, Y. Du, J. Hilton, L. Volokh, R. F. Dannals, J. J. Frost and J. M. Hare, *J. Nucl. Med.*, 2006, **47**, 1359–1366.
36 D. Y. Kim, H. S. Kim, H. Y. Jang, J. H. Kim, H. S. Bom and J. J. Min, *ACS Med. Chem. Lett.*, 2014, **5**, 1124–1128.
37 M. Zahid and P. D. Robbins, *Methods Mol. Biol.*, 2011, **683**, 277–289.
38 M. Zahid, B. E. Phillips, S. M. Albers, N. Giannoukakis, S. C. Watkins and P. D. Robbins, *PLoS One*, 2010, **5**, e12252.
39 D. Sahagun and M. Zahid, *Biomolecules*, 2023, **13**, 1690.
40 M. Zahid, K. S. Feldman, G. Garcia-Borrero, T. N. Feinstein, N. Pogodzinski, X. Xu, R. Yurko, M. Czachowski, Y. L. Wu, N. S. Mason and C. W. Lo, *Biomolecules*, 2018, **8**, 147.
41 K. S. Feldman and M. Zahid, *J. Visualized Exp.*, 2020, **160**, e60895.
42 M. Zahid, B. Weber, R. Yurko, K. Islam, V. Agrawal, J. Lopuszynski, H. Yagi and G. Salama, *Pharmaceutics*, 2023, **15**, 2107.
43 R. Yurko, K. Islam, B. Weber, G. Salama and M. Zahid, *Front. Chem.*, 2023, **11**, 1220573.
44 G. I. Gallicano, J. Fu, S. Mahapatra, M. V. R. Sharma, C. Dillon, C. Deng and M. Zahid, *Pharmaceuticals*, 2022, **15**, 871.
45 H. Kim, D. Mun, J. Y. Kang, S. H. Lee, N. Yun and B. Joung, *Mol. Ther. Nucleic Acids*, 2021, **24**, 1024–1032.
46 U. M. Avula, H. K. Yoon, C. H. Lee, K. Kaur, R. J. Ramirez, Y. Takemoto, S. R. Ennis, F. Morady, T. Herron, O. Berenfeld, R. Kopelman and J. Kalifa, *Sci. Transl. Med.*, 2015, **7**, 311ra172.
47 Y. J. Li, X. Hua, Y. Q. Zhao, H. Mo, S. Liu, X. Chen, Z. Sun, W. Wang, Q. Zhao, Z. Cui, T. An and J. Song, *Adv. Healthcare Mater.*, 2025, **14**, e2404068.
48 D. Kehr, J. Ritterhoff, M. Glaser, L. Jarosch, R. E. Salazar, K. Spaich, K. Varadi, J. Birkenstock, M. Egger, E. Gao, W. J. Koch, M. Sauter, M. Freichel, H. A. Katus, N. Frey, A. Jungmann, C. Busch, P. J. Mather, A. Ruhparwar,

M. Busch, M. Völkers, R. C. Wade and P. Most, *Circulation*, 2025, **151**(8), 548–565.
49 I. Ruseska and A. Zimmer, *Beilstein J. Nanotechnol.*, 2020, **11**, 101–123.
50 M. L. Chiu, J. F. Kronauge and D. Piwnica-Worms, *J. Nucl. Med.*, 1990, **31**, 1646–1653.
51 D. M. Chernoff, G. R. Strichartz and D. Piwnica-Worms, *Biochim. Biophys. Acta*, 1993, **1147**, 262–266.
52 J. C. Taubel, N. R. Nelson, A. Bansal, G. L. Curran, L. Wang, Z. Wang, H. M. Berg, C. J. Vernon, H. K. Min, N. B. Larson, T. R. DeGrado, K. K. Kandimalla, V. J. Lowe and M. K. Pandey, *Bioconjugate Chem.*, 2022, **33**, 892–906.
53 D. Faria, M. M. Herth, M. Konijnenberg, A. Korde, C. Kuntner-Hannes, R. M. Moresco, P. J. H. Scott, V. Shalgunov and S. Subramanian, *Guidance for Preclinical Studies with Radiopharmaceuticals*, IAEA Radioisotopes and Radiopharmaceuticals Series No. 8, International Atomic Energy Agency, IAEA, Vienna, 2023.
54 A. Todica, N. L. Beetz, L. Günther, M. J. Zacherl, U. Grabmaier, B. Huber, P. Bartenstein, S. Brunner and S. Lehner, *Mol. Imaging Biol.*, 2018, **20**, 268–274.
55 M. Fischer, M. J. Zacherl, L. Weckbach, L. Paintmayer, T. Weinberger, K. Stark, S. Massberg, P. Bartenstein, S. Lehner, C. Schulz and A. Todica, *Front. Cardiovasc. Med.*, 2021, **8**, 656742.
56 M. Fischer, T. Weinberger, D. Messerer, M. J. Zacherl, C. Schulz, S. Massberg, P. Bartenstein, S. Lehner, G. Boening and A. Todica, *Ann. Nucl. Med.*, 2022, **36**, 533–543.
57 A. S. L. Yu, A. S. L. Yu, G. M. Chertow, V. r. A. Luyckx, P. A. Marsden, K. Skorecki and M. W. Taal, *Brenner & Rector's the kidney*, Elsevier, Philadelphia, PA, 11th edn, 2020.
58 M. Salerno and G. A. Beller, *Circ. Cardiovasc. Imaging*, 2009, **2**, 412–424.
59 A. Autio, S. Uotila, M. Kiugel, V. Kytö, H. Liljenbäck, N. Kudomi, V. Oikonen, O. Metsälä, S. Helin, J. Knuuti, A. Saraste and A. Roivainen, *J. Nucl. Cardiol.*, 2020, **27**, 891–898.
60 E. Berezin and A. A. Berezin, *Dis. Markers*, 2020, **2020**, 1215802.
61 S. A. Leancă, D. Crişu, A. O. Petriş, I. Afrăsânie, A. Genes, A. D. Costache, D. N. Tesloianu and I. I. Costache, II, *Life*, 2022, **12**, 1111.
62 H. Houson, G. Nkepang, H. Gali and V. Awasthi, *J. Nucl. Med.*, 2018, **59**, 1534–1534.
63 G. N. Nkepang, H. Gali, H. Houson, A. F. Hedrick, B. Hayes, O. Causey, P. Inman, J. Box, E. Benton, W. Galbraith and V. Awasthi, *Appl. Radiat. Isot.*, 2019, **150**, 19–24.
64 H. M. Sherif, A. Saraste, E. Weidl, A. W. Weber, T. Higuchi, S. Reder, T. Poethko, G. Henriksen, D. Casebier, S. Robinson, H.-J. Wester, S. G. Nekolla and M. Schwaiger, *Circ. Cardiovasc. Imaging*, 2009, **2**, 77–84.
65 A. A. Ghotbi, A. Clemmensen, K. Kyhl, B. Follin, P. Hasbak, T. Engstrøm, R. S. Ripa and A. Kjaer, *J. Nucl. Cardiol.*, 2019, **26**, 798–809.